Structural and Electrical Properties of Thick κ-Ga_2O_3 Grown on GaN/sapphire Templates

A.Y. Polyakov[1], V. I. Nikolaev[2, 3], A.I. Pechnikov[2,3], S.I. Stepanov[2,3], E.B. Yakimov[1, 4], M.P. Scheglov[2], I.V. Shchemerov, [1], A.A. Vasilev[1], A.A. Kochkova[1], A.V. Chernykh[1], A.V. Chikiryaka[2] and S.J. Pearton[5]

[1] National University of Science and Technology MISiS, Moscow, Leninsky pr. 4, Moscow 119049, Russia

[2] Ioffe Physico-Technical Institute, 26 Polytekhnicheskaya Str., St. Petersburg 194021, Russia

[3]Perfect Crystals LLC, 28 Politekhnicheskaya str., 194064 St. Petersburg, Russia

[4]Institute of Microelectronics Technology and High Purity Materials, Russian Academy of Sciences, 6 Academician Ossipyan str., Chernogolovka, Moscow Region 142432, Russia

[5]Department of Materials Science and Engineering, University of Florida, Gainesville, FL 32611

ABSTRACT

Thick (23 μm) films of κ-Ga_2O_3 were grown by Halide Vapor Phase Epitaxy (HVPE) on GaN/sapphire templates at 630°C. X-ray analysis confirmed formation of single-phase κ-Ga_2O_3 with half-widths of the High-Resolution X-ray Diffraction (004), (006), (008) symmetric reflections of 4.5 arcminutes, and of asymmetric (027) reflection of 14 arcminutes. Orthorhombic κ-Ga_2O_3 polymorph formation was confirmed from analysis of the Kikuchi diffraction pattern in Electron Backscattering Diffraction. Secondary Electron imaging indicated a reasonably flat surface morphology with a few (area density ~10^3 cm^{-2}) approximately circular (diameter ~50-100 μm) uncoalesced regions, containing κ-Ga_2O_3 columns with in-plane dimensions and height about 10 μm. Micro-cathodoluminescence (MCL)spectra showed a wide 2-3.5 eV band that could be deconvoluted into narrower bands peaked at 2.59, 2.66, 2.86 and 3.12 eV. Ni Schottky diodes prepared on the films showed good rectification, but a high series resistance. The films had a thin near-surface region dominated by E_c-0.7 eV deep centers, and deeper region (~2 μm from the surface) dominated by shallow donors with concentration ≤ 10^{16} cm^{-3}. Photocurrent and photocapacitance spectra showed the presence of deep compensating

acceptors with optical ionization energy ~ 1.35 eV and 2.3 eV, the latter close to the energy of one of the MCL bands. Deep Level Transient Spectroscopy revealed deep traps with energies near 0.3, 0.6, 0.7, 0.8, 1 eV from the conduction band edge. The results show the potential of HVPE to grow very thick κ-Ga_2O_3 on GaN/Sapphire templates.

I.INTRODUCTION

Ga_2O_3 and related solid solutions are creating interest due to their wide bandgaps around 5 eV, controlled n-type doping, reasonable electron mobilities and saturation velocities and high photosensitivity in the far-UV spectral region. These properties make these materials promising for new generation high-power devices and solar-blind UV photodetectors [1-13]. So far, the studies have mostly focused on the thermodynamically stable β-polymorph, for which growth from the melt of large diameter, high quality bulk crystals suitable as substrates for epitaxial growth of device structures has been demonstrated [1-5]. However, metastable polymorphs of α-Ga_2O_3 with corundum structure and κ-Ga_2O_3 with orthorhombic structure are also attracting attention due to advantages they offer in comparison with the monoclinic β-polymorph [14-16].

The second most stable phase is believed to be the ε-polymorph (bandgap ~4.6 eV), often referred to as the κ-phase, which is thermodynamically stable up to 700 ˚C and converts to the β-phase above 900°C [8,10-14,17-23]. This has a pseudo-hexagonal crystal structure, ie. orthorhombic with 120˚ oriented domains. Cora et al.[24] reported this κ-Ga_2O_3 structure is ordered in 5–10 nm large domains, with each having orthorhombic structure with $Pna2_1$ space group symmetry. This orthorhombic κ-Ga_2O_3 is an ordered subgroup of the hexagonal ε-Ga_2O_3 phase, deriving from the arrangement of Ga atoms between the O planes. In κ-Ga_2O_3 the oxygen positions form with 4H (ABAC) close-packed stacking, with Ga^{3+} atoms occupying octahedra and tetrahedra that form two types of polyhedral layer parallel to the (001) direction [23-29]. The interest in κ-Ga_2O_3 arises from its high spontaneous polarization, up to an order of magnitude higher than in the III-Nitrides and thus the possibility of achieving a very high-density two-dimensional electron gas in heterojunction High Electron Mobility Transistors. These could provide an advance on their AlGaN/GaN analogs [14].

To date, growth of κ-Ga_2O_3 films has been reported at temperatures between 600ºC and 700ºC on flat and patterned sapphire, GaN and SiC by Halide Vapor Phase Epitaxy (HVPE) [17-20], mist Chemical Vapor Deposition (mist CVD) [21], Molecular Beam Epitaxy (MBE) [22],

Metalorganic Chemical Vapor Deposition (MOCVD) [23] and finally, by Pulsed Laser Deposition (PLD) on sapphire and ZnO [26]. The full potential of the κ-Ga_2O_3 polymorph has not been realized because of the unoptimized crystalline quality of the grown films. The tendency of κ-Ga_2O_3 to form 120° rotational domains with high dislocation density between the grains hampers the in-plane conductance in the films [26-29]. Because of this, films with such rotational domains have sometimes been believed to belong to a separate quasi-hexagonal ε-phase [27], although detailed x-ray and transmission electron microscope studies have unambiguously confirmed the orthorhombic symmetry of the κ-Ga_2O_3 epilayers [27,28]. Electrical, optical and luminescent properties of κ-Ga_2O_3 films [29,30] showed the presence of a broad micro cathodoluminescence (MCL) (2-3.2) eV band that could be deconvoluted into 4 peaks near 2.4 eV, 2.75 eV, 3 eV, 3.15 eV. These were attributed to acceptor centers in the lower half of the bandgap [29, 30]. The formation of κ-Ga_2O_3 films, of solid solutions of κ-Ga_2O_3 with Al, and of heterojunctions and quantum wells of κ-$(Al_xGa_{1-x})_2O_3/Ga_2O_3$ in PLD growth has been demonstrated [26,31], as well as their optical properties and the electrical properties of vertical structures grown on conducting ZnO [26].

Recently it has also been shown that the transformation of the β-Ga_2O_3 phase into the metastable κ-Ga_2O_3 phase can occur during high dose ion implantation, which creates a high density of radiation defects and strain. These are presumably conducive to the β-to-κ phase transition [32-34]. When growing Ga_2O_3 films on substrates with a large lattice mismatch, such as GaN, SiC [30] or diamond [35], the κ-Ga_2O_3 phase is often formed either alongside β-Ga_2O_3 or separately [30, 35]. In masked Epitaxial Lateral Overgrowth (ELOG) of α-Ga_2O_3 on sapphire, the initiation of κ-Ga_2O_3 phase has been observed at the edges of the wing regions when the thickness of the films and the strain increased [36].

In HVPE growth on patterned sapphire substrates, preferential κ-Ga_2O_3 formation has been reported for the valley regions and, when growth was performed at temperatures exceeding ~570°C, the entire upper portion of the films was κ-Ga_2O_3 [17-19, 30]. Growth on m-sapphire

substrates tends to promote the formation of the κ-polymorph [26, 31]. Recently, κ-Ga_2O_3 epitaxial films with strongly suppressed rotational domains formation have been prepared by ELOG in HVPE [37]. Single domain κ-Ga_2O_3 layers growth by mist CVD on ε-$GaFeO_3$ substrates has also been very recently reported [38]. Hence, the structural quality of κ-Ga_2O_3 films is improving due to the diligent work of multiple research groups. However, little is known about the spectra of electronic states in very thick κ-Ga_2O_3 with improved crystal quality. In this paper, we report trap studies performed for Ni Schottky diodes deposited on thick κ-Ga_2O_3 films grown by HVPE on GaN-on-sapphire templates. Increasing the thickness improves film quality of the upper portions of the layer comparable to those obtained by ELOG [37].

II.EXPERIMENTAL

The samples were grown in a homemade atmospheric horizontal quartz HVPE reactor described elsewhere [18,19,20,30]. The growth was done using GaCl (formed in-situ by passing HCl over the Ga-containing boat) and spectrally clean O_2 as precursors (the mole ratio of the O_2 to Ga flows was 3.1). The substrates were 4-μm-thick unintentionally doped GaN films deposited by HVPE on basal plane sapphire. The growth temperature was 630°C, the growth rate was 1.6 μm/h and the overall thickness of the Ga_2O_3 layers was 23 μm. The reason the growth was performed on GaN-on-saphire template rather than on sapphire is as follows. Single-phase growth of κ-Ga_2O_3 on sapphire is tricky: at lower growth temperatures between 500°C and 650°C, growth is highly sensitive to the sapphire substrate orientation and tends to be a mixture of the α-Ga_2O_3 and κ-Ga_2O_3 polymorphs for growth on planar basal plane substrates, but growth on r-plane and m-plane sapphire tends to stabilize growth of α-polymorph, whereas, for patterned (0001) substrates, the nucleation of the κ-polymorph occurs mostly on the tips of the cones of the pattern and the overall growth result is very sensitive to the growth temperature. At higher growth temperature the competition with β-Ga_2O_3 becomes an issue ([12, 17, 18, 30, 31]). At the same time, the nucleation and persistence of the κ-phase is very sensitive to strain [12, 17, 18, 26, 30, 31], and the κ-polymorph is preferably deposited on cubic, wurtzite, hexagonal

substrates at temperatures up to 650ºC [12, 17, 18, 19]. This makes obtaining single-phase κ-Ga_2O_3 films more straightforward. Besides, combining κ-Ga_2O_3 with III-Nitrides could have interesting features due to both materials having high spontaneous electrical polarization that can lead in principle to the formation of two-dimensional electron and hole gases at the interfaces.

The phase composition of the layers was determined from X-ray Diffraction (XRD), using Cu_{Ka1} radiation. The crystalline quality was also analyzed by measuring the Full Width at Half Maximum (FWHM) of High-Resolution X-ray Diffraction (HRXRD) symmetric and asymmetric reflections in triple-axis geometry. The morphology of the surface was analyzed by observation in the secondary electron mode (SE) of a Scanning Electron Microscope (SEM) JSM-6490 (JEOL, Japan). This SEM was equipped with an Oxford Instruments HKL Nordlys EBSD camera (acquisition and evaluation software Channel5), which was also employed to perform Electron Backscatter Diffraction (EBSD) measurements to determine the crystal symmetry and orientation [39]. Micro-cathodoluminescence (MCL) spectra were measured at room temperature using a MonoCL-3 (Gatan, UK) system with Hamamatsu photomultiplier as a detector. The charge carrier recombination efficiency was characterized by Electron Beam Induced Current (EBIC) [19, 40].

For electrical and deep trap characterization, semi-transparent 20-nm thick Ni Schottky diodes of 1.2 mm in diameter were deposited via e-beam evaporation through a shadow mask. Ohmic contacts were formed by e-beam deposition through a shadow mask of Ti/Au bilayer (20 nm/80 nm) [19, 20]. Characterization included current-voltage (I-V), capacitance- frequency (C-f) and capacitance-voltage (C-V) measurements performed in the dark and under monochromatic illumination with a set of high-power light emitting diodes (LEDs) with peak wavelengths from 365 nm to 950 nm and optical output power 250 mW/cm^2. For above-bandgap excitation in these measurements, three parallel 259 nm wavelength LEDs with total output power 1.2 mW/cm^2 were used. The C-V and C-f data were measured with monochromatic optical excitation, ie. LCV [18,19, 27] and photocapacitance [18,19,41]) used to determine the optical emission

spectra of traps. The deep trap spectra were determined from admittance spectra (AS) and Deep Level Transient Spectroscopy with electrical (DLTS) or optical (ODLTS) injection [42]. All these measurements were performed in the temperature range of 77-500K [19,20, 41].

III.RESULTS AND DISCUSSION

The results of XRD θ–2θ measurements are presented in Fig.1. The main peaks observed are the κ-Ga_2O_3 (002), (004), (006), (008), (0010) reflections from the (001) plane and the reflections from the GaN/Al_2O_3 substrate. The HRXRD rocking curves half-width measurements for the symmetric (004), (006), (008) reflections gave the FWHM values of 4.5'. For asymmetric (027) reflection, the FWHM value was 14'.

A typical backscatter Kikuchi diffraction pattern is displayed in Fig. 2 (a). The results of the band identification in this diffraction pattern performed using the Hough transform [39] are displayed in Fig. 2(b) and confirm that the film is κ-Ga_2O_3. These observations prove a single-phase κ-Ga_2O_3 layer has been formed, with good crystalline quality.

SE images of the surfaces show that, alongside the reasonably flat surface, there existed regions with growing grains not fully merged and formed by large, partly rectangular, partly hexagonal features with characteristic in-plane dimension and height of ~ 10 μm (Fig. 3, see also a higher magnification Fig. S1(a) in the Supplementary Material). In EBIC images, these uncoalesced regions produced a bright contrast coming mainly from the sidewalls of the columns, whereas the EBIC signal for the flat portion of the surface was low. This implies a strong recombination in the top region of the (001) growth surface related to presence of a high density of deep states near the surface. The recombination on the sidewalls was not strongly suppressed so that they appeared bright in EBIC images (Fig. S1(a,b) of the Supplementary Material compares the SE and EBIC images of a not fully overgrown region with columns).

A MCL spectrum measured on the flat portion of the film is shown in Fig. 4. The spectral shape is quite similar to that observed [17] for κ-Ga_2O_3 film prepared by MOCVD and ascribed to several deep acceptor levels in the lower half of the bandgap. A similar MCL band has been

described [30] for films grown by HVPE. As in Ref. [17], the 2-3.5 eV MCL band could be accurately fitted with 4 Gaussian bands peaked at 2.59, 2.66, 2.86 and 3.12 eV (Fig. 4 displays the experimental spectrum and the results of fitting). The peak energies are close, but slightly different from those reported in Ref. [29]. Local MCL spectra measurements on the flat tops of columns in the not fully overgrown regions did not differ from the spectrum shown in Fig. 4.

I-V characteristics of the Ni Schottky diodes are displayed for three temperatures of 130K, 296K, 420K in Fig. 5. In all cases, the rectification was high, the leakage current was low, but the ideality factor was 2.6 at room temperature and 1.8 at 420K, accompanied by high series resistance. The activation energy from temperature dependence of the forward current at 2V (the region of saturation with voltage due to the series resistance) was 0.3 eV (Fig. S2 of the Supplementary Material). The samples showed a high photosensitivity, particularly for above-bandgap excitation with the 259 nm LED (Fig. 6 (a); for LED wavelengths up to 365 nm the optical output power density was 250 mW/cm^2 while for the 259 nm LED it was 1.2 mW/cm^2 which converts to photosensitivity of about 0.02 A/W and a rejection factor higher than 1000 for the visible-near-UV light. Figure 6 (b) shows the spectral dependence of the forward current.

C-f characteristics for 130K, 296K, and 420K measured at 0 V are compared in Fig. 7(a). The frequency dependence at high temperature displays two plateaus indicating the presence of two types of centers determining the overall capacitance at low and high probing frequencies. C-V profiling at frequencies corresponding to the low-frequency and high frequency plateaus allowed determination of the spatial distribution and concentration of these centers. For the low-frequency C-f plateau, the concentration was N_T=1.2×10^{17} cm^{-3} and these centers were located in a rather shallow region (see S3 in Supplementary material). When the measurements were performed at 100 kHz corresponding to the high-frequency plateau, the films showed full depletion of the centers responding at this frequency down to a depth of 1.8 μm and only at higher depth a measurable concentration of ~10^{16} cm^{-3} appeared (Figures S3(a, b) of the Supplementary material show respective 1/C^2 versus V plots and S4 shows the carrier profile).

Measurement of the temperature dependence of the capacitance derivative with temperature, dC/dT, for different low frequencies gave a set of peaks whose temperature position shifted to higher values with increasing frequency (Fig. 7(b)). This allows determination of the depth of the peak in respect to the conduction band, E_a, and the electron capture cross section, σ_n, from the equation of the admittance spectroscopy $1/e_n(T_M)=1/(2\pi f)$ [28], where $e_n(T_M)$ is the electron emission rate from the deep trap at the temperature of the peak T_M corresponding to the measurement frequency. This analysis gives the ionization energy of the traps determining the width of the space charge region (SCR) and hence the capacitance as E_a=0.7 eV and the electron capture cross section as $\sigma_n=10^{-15}$ cm^2.

At high frequency corresponding to the high-frequency plateau in C-f, the 0.7 eV deep traps near the surface do not respond to the probing frequency in C-V profiling and the region where such centers dominate behaves as a capacitance of a dielectric layer switched in series with the region where the Fermi level is pinned by shallow centers that can respond to probing frequency [42]. Hence, the capacitance at this frequency is lower [28]. In C-V profiling at this frequency we see that the layers are depleted to about 1.8 μm and only for higher depths start to depend on applied voltage. This is manifested by the $1/C^2$-V plot being non-linear and the apparent voltage offset being high, over 22 V. The net concentration of these shallower donors on which the Fermi level is pinned deep inside the films is ~ 6×10^{15} cm^{-3} at 1.8 μm and slowly grows deeper into the sample. The depth of these centers could not be determined from admittance spectroscopy, but the temperature dependence of the forward current in I-V characteristics serve as a measure of the activation energy of the centers, ~ 0.3 eV.

The balance between the deep 0.7 eV traps, the 0.3 eV traps, and deep compensating acceptors, determines the position at which the Fermi level is pinned. The type and density of these compensating centers can be determined from photocapacitance ΔC_{ph} spectra. Fig. 8(a) displays the $2N_T\Delta C_{ph}/C_{dark}$ spectrum obtained at 0V and 20 Hz (N_T is the net concentration of the 0.7 eV traps determining the space charge width in low-frequency C-V profiling, C_{dark} is the dark

capacitance at 0V and 20 Hz). This value allows to approximately determine the concentration of deep acceptors compensating conductivity [42]. The spectrum shows two optical thresholds near 1.35 eV and 2.3 eV similar to those seen in photocurrent spectra in forward current. The concentration of these compensating acceptors is ~ 10^{16} cm^{-3} for the 1.35 eV centers and 7.8×10^{16} cm^{-3} for the centers with optical ionization threshold near 2.3 eV.

For capacitance frequency of 100 kHz, the photocapacitance spectra showed the same optical thresholds, but the concentrations of respective deep traps calculated using the donor concentration close to 6×10^{15} cm^{-3} from the concentration profile were, respectively, 4×10^{14} cm^{-3} and 10^{15} cm^{-3}, i.e. the concentrations of compensating acceptors increased about two orders of magnitude towards the surface.

Deep level spectroscopy is not straightforward in nonuniform samples, but at 100 kHz, assessment of the spectra was feasible in the region near 2 μm from the surface with pulsing from -2V to 1V when the space charge region boundary was swept from ~ 2.2 μm to 1.8 μm. This spectrum is presented in Fig.8(b). The y-axis in the figure is the product of $2N_d(\Delta C/C)F^{-1}$ (N_d is the concentration of donors determined from C-V profiling, ΔC is difference of capacitances at the time windows t1 and t2 in DLTS, C is the steady-state capacitance, F^{-1} is the DLTS spectrometer function converting ΔC to the total amplitude of the capacitance transient [42]). The abscissa values at the peak temperatures gives the densities of the traps without taking the λ-correction [28].This approach is often used to graphically compare the concentration of different traps in various DLTS spectra [27]). The presence of electron traps E1 ($E_a=E_c$-0.3 eV, $\sigma_n=1.5\times10\text{-}^{17}$ cm^2), E2(0.6 eV, $\sigma_n=1.2\times10^{-13}$ cm^2), E3(0.7 eV, $\sigma_n=3\times10^{-14}$ cm^2), E4(0.8 eV, $\sigma_n=2.5\times10^{-14}$ cm^2), E5(1 eV, $\sigma_n=1.8\times10^{-14}$ cm^2) were observed.

ODLTS spectra shown in Figure 8(b) and measured with optical excitation with above-bandgap light from the 259 nm LED and applied bias of -1V showed a superposition of the signal from the deep electron traps superimposed on a very broad hole-trap-like signal (compare DLTS and ODLTS spectra in Fig. S5(a, b) in the Supplementary Material). The DLTS signal

measured with long filling pulses displayed unusual wide negative hole-trap-like background whose magnitude became higher with increased pulse length. These phenomena are specific to Ga_2O_3 and have been also observed by us in some cases for β-Ga_2O_3 and α-Ga_2O_3 samples and is yet to be understood. A possible explanation could be the high depth of native acceptors and the existence of barriers for capture of electrons with these centers [16].

IV.SUMMARY AND CONCLUSIONS

We have shown that thick, single-phase κ-Ga_2O_3 films can be grown by HVPE on GaN at 630ºC. This is a consequence of the κ-Ga_2O_3 phase being promoted in preference to the α-polymorph which is produced at lower temperatures, when the high strain and temperatures over ~500ºC are involved [6]. For thick κ-Ga_2O_3 films grown at these conditions, the crystalline quality is comparable to that of films grown by ELOG [37]. The origin of uncoalesced κ-Ga_2O_3 regions need to be understood to suppress their formation. Even with their presence, Ni Schottky barriers showed low leakage current, allowed probing by steady-state and transient capacitance techniques, and showed a relatively high photosensitivity. In the top ~0.2 μm of the layers, the electrical properties were dominated by a high density of E_c-0.7 eV electron traps. Deeper inside the films, down to about 2 μm, there was compensation and the density of the charged centers capable to respond to high probing frequencies in C-f, C-V, AS measurements such that the films were depleted of charge carriers even at 0 V bias. Beyond this depth, the Fermi level was pinned by relatively shallow donors with concentration of ~6×10^{15} cm^{-3}.

Photocapacitance and photocurrent spectra show the compensating acceptors have optical ionization thresholds near 1.35 eV and 2.3 eV. The concentration of the main 2.3 eV trap decreases from 7.4×10^{16} cm^{-3} near the surface to 10^{15} cm^{-3} deep inside the films. DLTS spectra showed the existence of five deep traps E1 (Ea=E_c-0.3 eV), E2(0.6 eV), E3(0.7 eV), E4(0.8 eV), E5(1 eV) in the region below ~2 μm from the surface. The E3 traps seem to be the same as the E_c-0.7 eV traps detected in AS and their density increases towards the surface. The charge collection efficiency in EBIC was very low for flat regions of the grown surface, but greatly

increased at the sidewalls of the columns forming not completely merged surface regions in the film. This correlates with the fact the density of the E_c-0.7 eV electron traps and 2.3 eV hole traps strongly falls inside the films, suggesting that either could be effective lifetime killers. The spectra of deep traps detected in κ-Ga_2O_3 strongly resembles the spectra described for β-Ga_2O_3 and α-Ga_2O_3 polymorphs [16]. That is despite a considerable difference in the atomic arrangement in these three polymorphs. While detailed theoretical modeling results predicting the electronic structure and formation energy of defects in κ-Ga_2O_3 is absent, based on calculations performed for β-Ga_2O_3 and α-Ga_2O_3 [43, 44] the acceptors with levels at E_c-2.3 eV in our κ-Ga_2O_3 are likely related to gallium vacancies or their complexes. This would imply the surface of our films is Ga-deficient.

Future work will focus on understanding reasons for non-coalescence of the films and of the buildup of deep traps towards the surface. The goal is to suppress the strong recombination and trapping of charge carriers near the surface and improve the electrical performance and photosensitivity of Ni Schottky diodes on κ-Ga_2O_3. The ability to grow very thick κ-Ga_2O_3 on inexpensive templates allows for many options, including p-n heterojunctions.

Supplementary Material

See supplementary material for additional characterization results from the grown films.

Data Availability

The data that supports the findings of this study are available within the article and its supplementary material.

ACKNOWLEDGMENTS

The work at NUST MISiS was supported in part by the Russian Science Foundation, grant no. 19-19-00409. The work at IMT RAS was supported by the State Task No 075-00706-22-00. The work at UFL was performed as part of Interaction of Ionizing Radiation with Matter University Research Alliance (IIRM-URA), sponsored by the Department of the Defense, Defense Threat Reduction Agency under award HDTRA1-20-2-0002. The content of the information does not

necessarily reflect the position or the policy of the federal government, and no official endorsement should be inferred. The work was also supported by NSF DMR 1856662.

Conflicts of interest

The authors have no conflicts to disclose.

REFERENCES

1. S. J. Pearton, Fan Ren, Marko Tadjer, and Jihyun Kim, J. Appl. Phys. 124, 220901 (2018)

2. Gallium Oxide: Materials Properties, Crystal Growth, and Devices, ed. Masataka Higashiwaki and Shizuo Fujita (Springer Series in Materials Science, 2020).

3. Hongpeng Zhang, Lei Yuan, Xiaoyan Tang, Jichao Hu, Jianwu Sun, Yimen Zhang, Yuming Zhang and Renxu Jia, IEEE Trans. Power Electron. 35, 5157 (2020).

4. A. J. Green, J. Speck, G. Xing, P. Moens, F. Allerstam, K. Gumaelius, T. Neyer, A. Arias-Purdue, V. Mehrotra, A. Kuramata, K. Sasaki, S. Watanabe, K. Koshi, J. Blevins, O. Bierwagen, S. Krishnamoorthy, K. Leedy, A. R. Arehart, A. T. Neal, S. Mou, S. A. Ringel, A. Kumar, A. Sharma, K. Ghosh, U. Singisetti, W. Li, K. Chabak, K. Liddy, A. Islam, S. Rajan, S. Graham, S. Choi, Z. Cheng, and M. Higashiwaki, APL Mater. 10, 029201 (2022).

5. Kentaro Kaneko, Shizuo Fujita, and Toshimi Hitora, Jpn. J. Appl. Phys 57, 02CB18 (2018).

6. Kazuyuki Uno, Riena Jinno, and Shizuo Fujita, J. Appl. Phys. 131, 090902 (2022).

7. Joseph A. Spencer, Alyssa L. Mock, Alan G. Jacobs, Mathias Schubert, Yuhao Zhang and Marko J. Tadjer, Appl. Phys. Rev. 9, 011315 (2022).

8. M. Bosi, P. Mazzolini, L. Seravalli and R. Fornari, J. Mater. Chem. C, 8, 10975 (2020).

9. J. Xu, W. Zheng and F. Huang, J. Mater. Chem. C, 7, 8753 (2019).

10. M. Pavesi, F. Fabbri, F. Boschi, G. Piacentini, A. Baraldi, M. Bosi, E. Gombia, A. Parisini, R. Fornari, Mater. Chem. Phys. 205, 502 (2018).

11. F. Mezzadri, G. Calestani, F. Boschi, D. Delmonte, M. Bosi, R. Fornari, Inorg. Chem. 55, 12079 (2016).

12. Y. Oshima, E.G. Víllora, Y. Matsushita, S. Yamamoto, K. Shimamura, J. Appl. Phys. 118, 085301(2015).

13. H.J. von Bardeleben, J.L. Cantin, A. Parisini, A. Bosio, R. Fornari, Phys, Rev. Mater. 3, 084601(2019).

14. M. B. Maccioni, and V. Fiorentini, Appl. Phys. Express 9, 041102 (2016).

15. Elaheh Ahmadi, and Yuichi Oshima, J. Appl. Phys. 126, 160901 (2019).

16. A. Y. Polyakov, V. I. Nikolaev, E. B. Yakimov, F. Ren, S. J. Pearton, and J. Kim, J. Vac. Sci. Technol. A 40, 020804 (2022).

17. V. I. Nikolaev, A. I. Pechnikov, V. V. Nikolaev, M. P. Scheglov, A.V. Chikiryaka, S. I. Stepanov, O. S. Medvedev, S. V. Shapenkov, E. V. Ubyivovk and O. F. Vyvenko, J. Physics: Conference Series1400, 055049 (2019).

18. V. I. Nikolaev, S. I. Stepanov, A. I. Pechnikov, S.V. Shapenkov, M. P. Scheglov, A.V. Chikiryaka, and O. F. Vyvenko, ECS J. Solid State Sci. Technol., 9, 045014 (2020).

19. A. Y. Polyakov, V. I. Nikolaev, S. I. Stepanov, A. I. Pechnikov, E. B. Yakimov, N.B. Smirnov, I. V. Shchemerov, A. A. Vasilev, A. I. Kochkova, A.V. Chernykh, and S.J. Pearton, ECS J. Solid State Sci. Technol, 9, 045003(2020).

20. A. Y. Polyakov, N. B. Smirnov, I. V. Shchemerov, E. B. Yakimov, V. I. Nikolaev, S. I. Stepanov, A. I. Pechnikov, A. V. Chernykh, K. D. Shcherbachev, A. S. Shikoh, A. Kochkova, A. A. Vasilev, and S. J. Pearton, APL Mater. 7, 051103 (2019)

21. S. Yusa, D. Oka, and T. Fukumura, CrystEngComm 22, 381 (2020).

22. M. Kracht, A. Karg, J. Schörmann, M. Weinhold, D. Zink, F. Michel,M. Rohnke, M. Schowalter, B. Gerken, A. Rosenauer, P. J. Klar, J. Janek, and M. Eickhoff, Phys. Rev. Appl. 8, 054002 (2017).

23. A. Parisini, A. Bosio, V. Montedoro, A. Gorreri, A. Lamperti, M. Bosi,G. Garulli, S. Vantaggio, and R. Fornari, APL Mater. 7, 031114 (2019).

24. I. Cora, F. Mezzadri, F. Boschi, M. Bosi, M. Caplovicova, G. Calestani, I. D´odony, B. P´ecz, R. Fornari, Cryst. Eng. Commun. 19, 1509 (2017).

25. R. Fornari, M. Pavesi, V. Montedoro, D. Klimm, F. Mezzadri, I. Cora, B. Pecz, F. Boschi, A. Parisini, A. Baraldi, C. Ferrari, E. Gombia, M. Bosi, Acta Mater. 140, 411 (2017).

26. M. Kneiß, D. Splith, P. Schlupp, A. Hassa, H. von Wenckstern, M. Lorenz, and M. Grundmann, J. Appl. Phys. 130, 084502 (2021).

27. I. Cora, Zs. Fogarassy , R. Fornari , M. Bosi , A. Recnik , B. Pécz, Acta Materialia 183, 216 (2020).

28. H. von Wenckstern, Adv. Electron. Mater. 3, 1600350 (2017).

29. V. Montedoro, A. Torres, S. Dadgostar, J. Jimenez, M. Bosi, A. Parisini, R. Fornari, Materials Sci. Engineering B 264, 114918 (2021).

30. Sevastian Shapenkov, Oleg Vyvenko, Vladimir Nikolaev, Sergei Stepanov, Alexei Pechnikov, Mikhail Scheglov, and Georgiy Varygin, Phys. Status Solidi B 2021, 2100331

31. A. Hassa, C. Wouters, M. Kneiß, D. Splith, C. Sturm, H. von Wenckstern, M. Albrecht, M. Lorenz and M. Grundmann, J. Phys. D: Appl. Phys. 53, 485105 (2020).

32. Alexander Azarov, Calliope Bazioti, V. Venkatachalapathy, P. Vajeeston , Edouard Monakhov, and Andrej Kuznetsov, Phys. Rev. Lett. 128, 015704 (2022).

33. D. Tetelbaum, A. Nikolskaya, D. Korolev, T. Mullagaliev, A. Belov, V. Trushin, Y. Dudin, A. Nezhdanov, A. Mashin, A. Mikhaylov, A. Pechnikov, M. Scheglov, V. Nikolaev, and D. Gogova, Materials Letters 302, 130346 (2021).

34. E. A. Anber, D. Foley, A. C. Lang, J. Nathaniel, J. L. Hart, M. J. Tadjer, K. D. Hobart, S. Pearton, and M. L. Taheri, Appl. Phys. Lett. 117, 152101 (2020).

35. A. Y. Polyakov, V. I. Nikolaev, S. A. Tarelkin, A. I. Pechnikov, S. I. Stepanov, A. E. Nikolaev, I. V. Shchemerov, Eugene B. Yakimov, Nikolay V. Luparev, M. S. Kuznetsov, A. A.Vasilev, A. I. Kochkova, M. I. Voronova, M. P. Scheglov, J. Kim, and S. J. Pearton, J. Appl. Phys. 129, 185701 (2021)

36. Y. Oshima, K. Kawara, T. Shinohe, T. Hitora, M. Kasu, and S. Fujita, APL Materials 7, 022503 (2019).

37. Y. Oshima, K. Kawara, T. Oshima, and T. Shinohe, Japan J. Appl. Phys. 59, 115501 (2020)

38. Hiroyuki Nishinaka, Osamu Ueda, Yusuke Ito, Noriaki Ikenaga, Noriyuki Hasuike, and Masahiro Yoshimoto, Japan. J. App. Phys. 61, 018002 (2022)

39. K. Z. Baba-Kishi, J. Mater. Sci. 37, 1715 (2002).

40. E. B. Yakimov, A. Y. Polyakov, N. B. Smirnov, I. V. Shchemerov, P. S. Vergeles, E. E. Yakimov, A. V. Chernykh, Minghan Xian, F. Ren and S. J. Pearton, J. Phys. D: Appl. Phys. 53, 495108 (2020).

41. A. Y. Polyakov, N. B. Smirnov, I. V. Shchemerov, S. J. Pearton, F. Ren, A. V. Chernykh, P. B. Lagov and T. V.Kulevoy, APL Materials 6, 096102 (2018)

42. Capacitance spectroscopy of semiconductors, ed. Jian V. Li and Giorgio Ferrari (Pan Stanford Publishing Pte Ltd, Singapore, 2018) 437 pp.

43. M. E. Ingebrigtsen, A. Y. Kuznetsov, B. G. Svensson, G. Alfieri, A. Mihaila, U. Badstubner, A. Perron, L. Vines, and J. B. Varley, APL Mater. 7, 022510 (2019).

44. T. Kobayashi, T. Gake, Yu Kumagai, F. Oba and Y. Matsushita, Appl. Phys. Express 12, 091001 (2019).

FIGURE CAPTIONS

Fig. 1(Color online) XRD pattern of κ-Ga_2O_3 films; there are 5 strong reflections (002), (004), (006), (008), (0010) of the (001) κ-Ga_2O_3 planes and reflections due to the GaN-on–basal plane sapphire (GaN/Al_2O_3); the low amplitude reflections for out-of-plane κ-Ga_2O_3 facets are likely owing to the reflections from the sidewalls of columns in the uncoalesced κ-Ga_2O_3 regions.

Fig. 2(Color online) (a) typical backscatter Kikuchi diffraction pattern for κ-Ga_2O_3 films; (b) illustration of the band indentification for Kikuchi diffraction pattern by the Hough transform.

Fig. 3. Secondary electron image of the uncoalesced part of the surface with columnar features, the sample is inclined by 70^o in respect to the probing electron beam.

Fig. 4 (Color online) Typical 300K MCL spectrum obtained with beam energy of 10 keV and current of 0.1 nA (blue open circles). The spectrum consists of a broad band in the spectral range 2–3.5 eV and can be fitted by four Gaussian bands centered at 2.59, 2.66, 2.86 and 3.12 eV. The bands and the resultant simulated spectrum are shown with magenta lines.

Fig. 5. (Color online)I-V characteristics of Ni Schottky diodes on the κ-Ga_2O_3; measurements at 130K (blue line), 297K (black line), 420K (red line).

Fig. 6 (Color online) (a) 300K I-V characteristics in the dark (black line) and under illumination (the data shown for the 250 mW/cm^2 LEDs excitation with wavelength of 940 nm (magenta line), 660 nm (red line), 530 nm (olive line),400 nm (blue line), 365 nm (violet line) and for 1.2 mW/cm^2 259 nm LED (orange line); (b) spectral dependence of forward current at 2 V.

Fig. 7 (Color online) (a) The dark C-f dependences at 130K, 297K, and 420K measured at 0V; (b) the spectral dependence of $2N_T\Delta C_{ph}/C_{dark}$ at 420K at 20 Hz

Fig. 8(a) (Color online)The derivative dC/dT calculated from high-temperature C-T measurements at 0V; data shown for frequencies f= 20, 30, 50, 100, 200 Hz, Arrhenius analysis of characteristic relaxation time corresponding to temperature of the peak, $\tau=1/(2\pi f)$ gives activation energy as E_a=0.7 eV and $\sigma_n=10^{-15}$ cm^2. (b) (Color online) DLTS spectrum of κ-Ga_2O_3 at 100 kHz, at bias of -2V, forward bias pulse 1V (50 ms), time windows t_1/t_2=1.5 s/15 s.

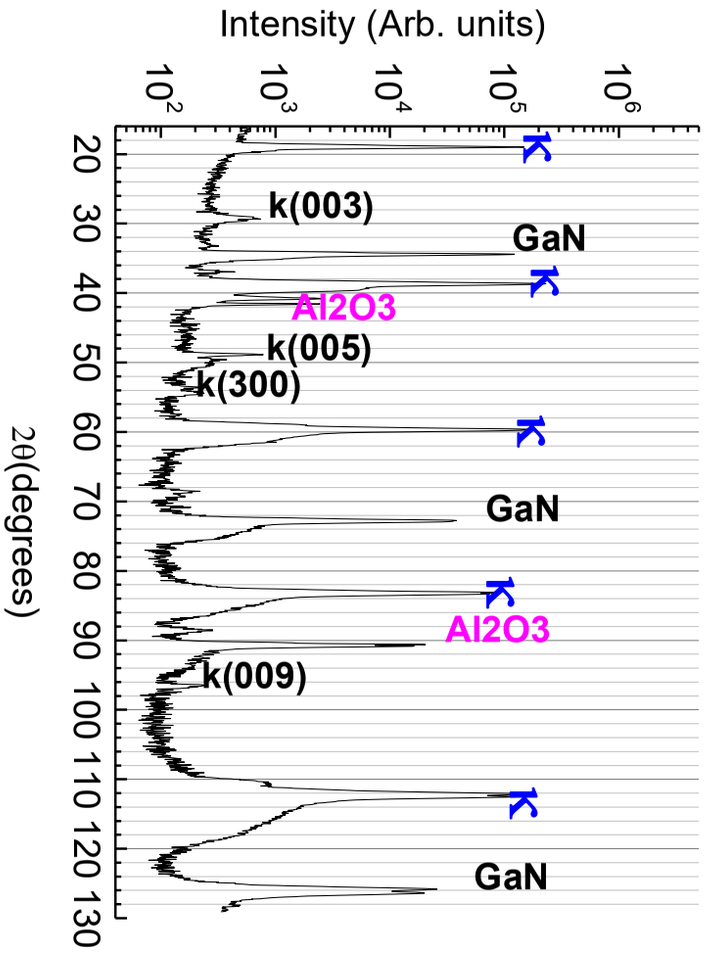

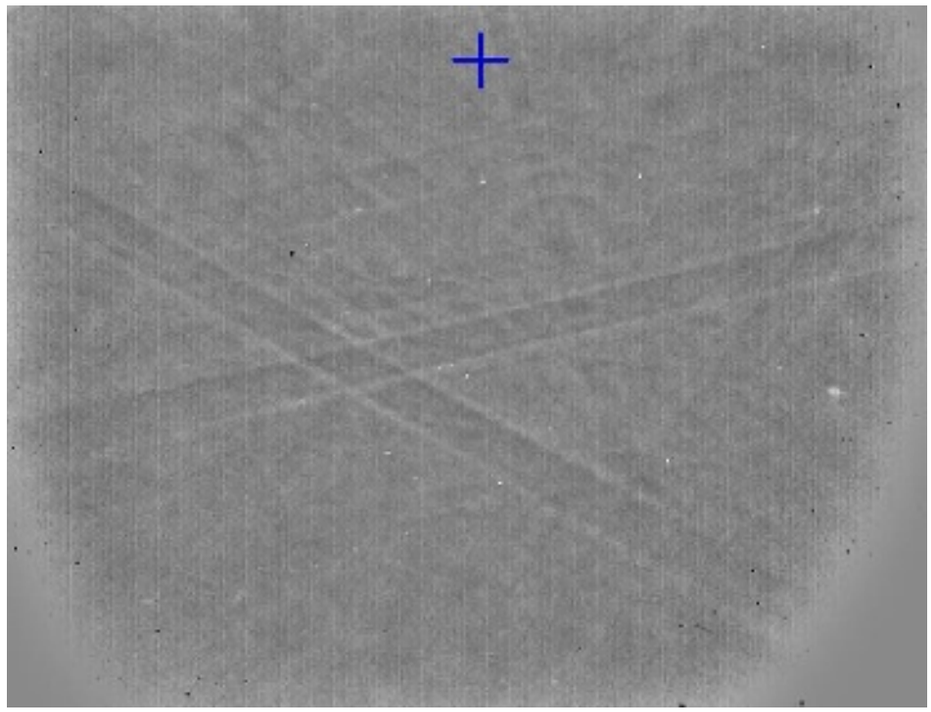

(a)

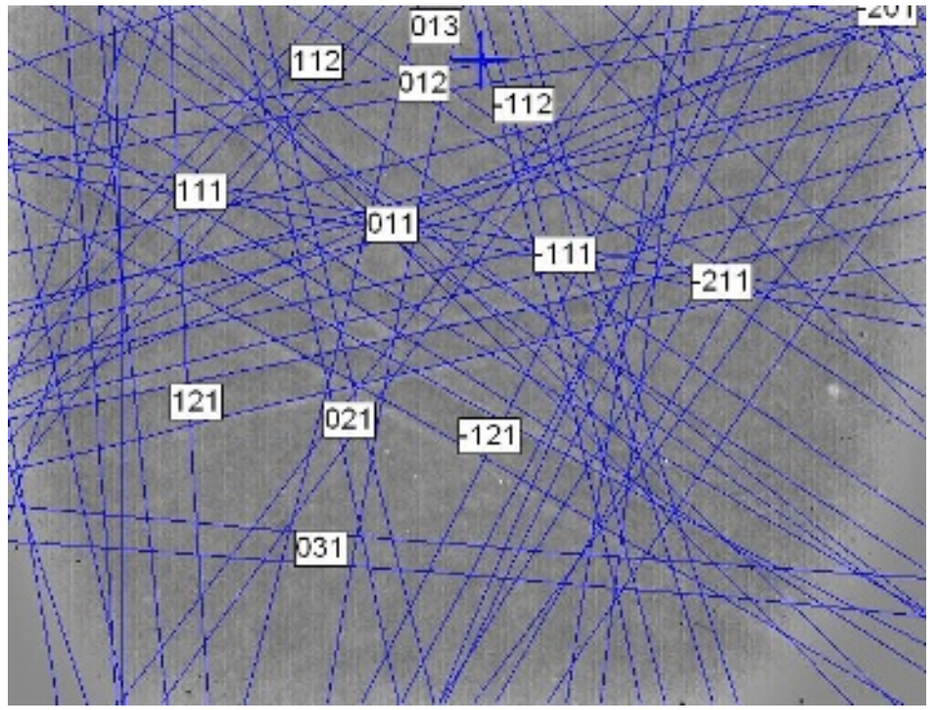

(b)

PLEASE CITE THIS ARTICLE AS DOI:10.1063/5.0091653

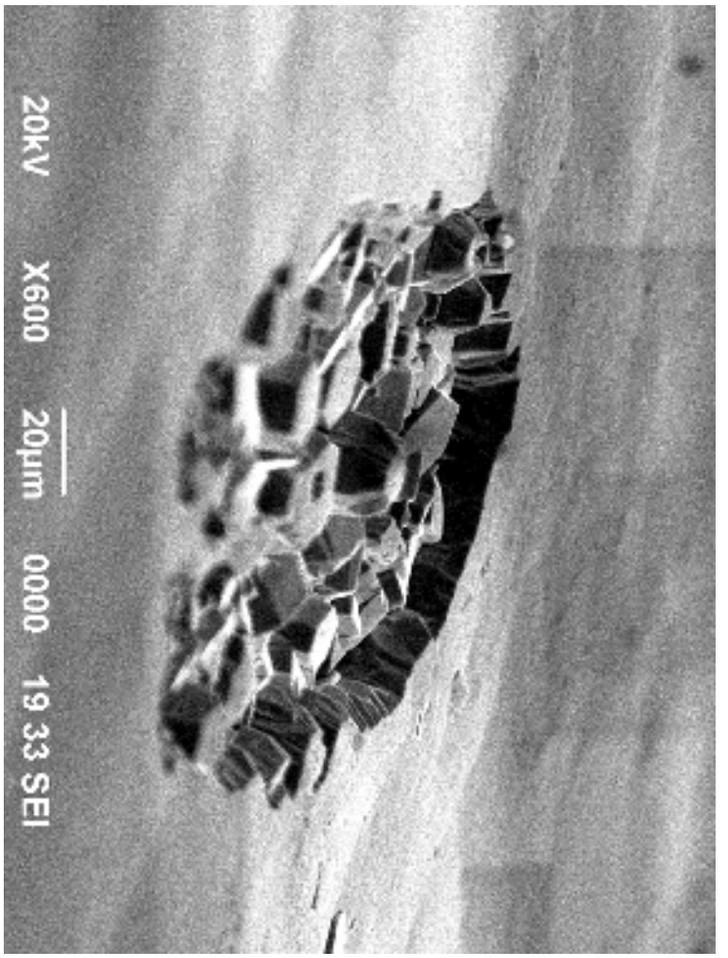

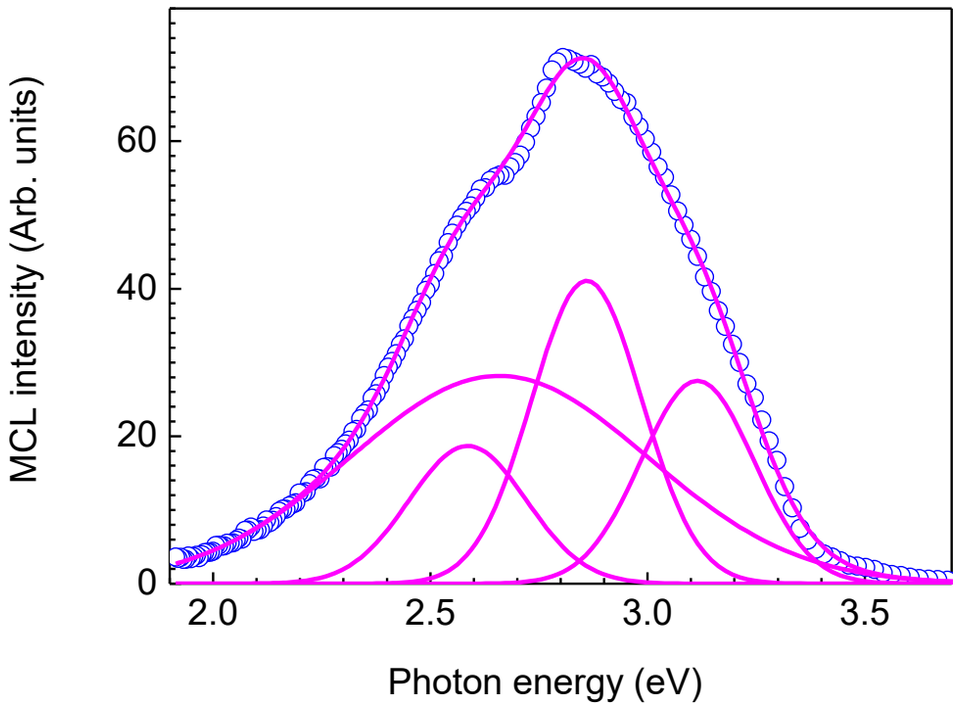

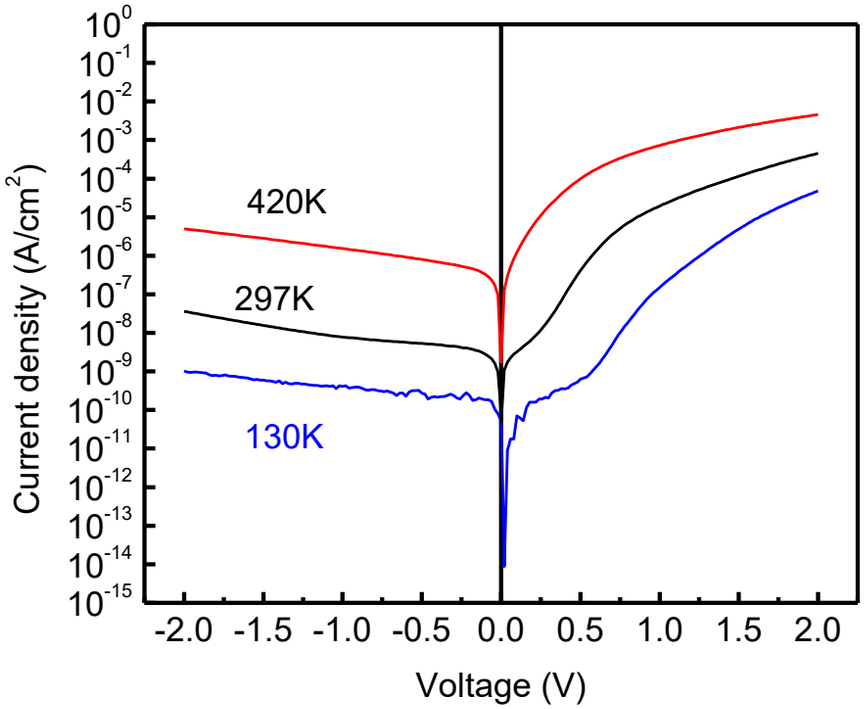

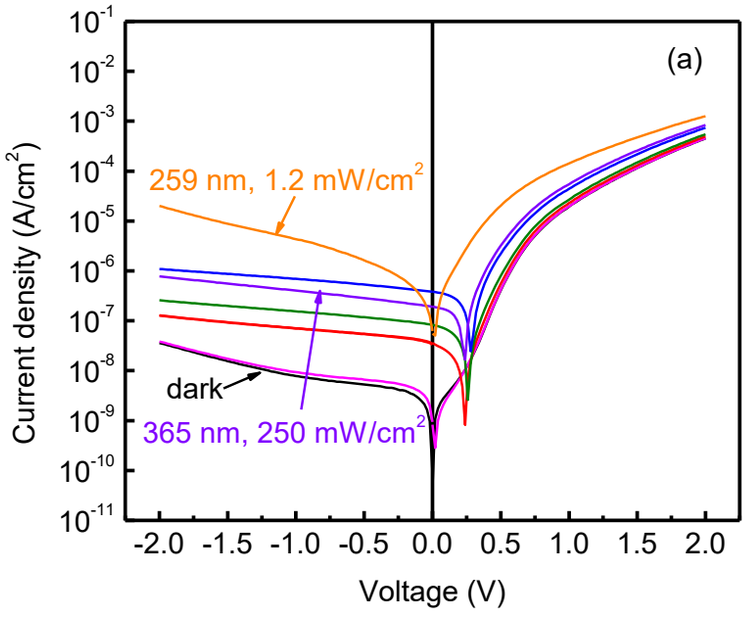

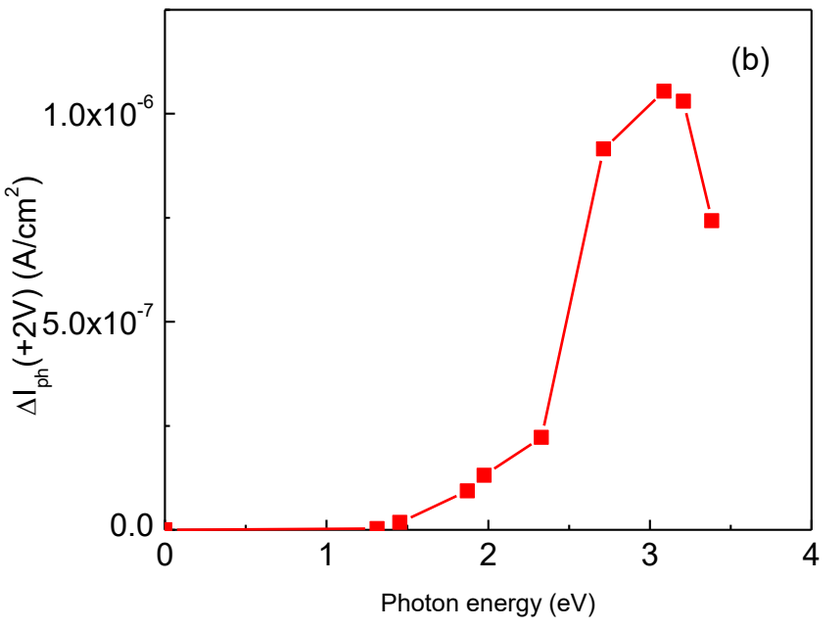

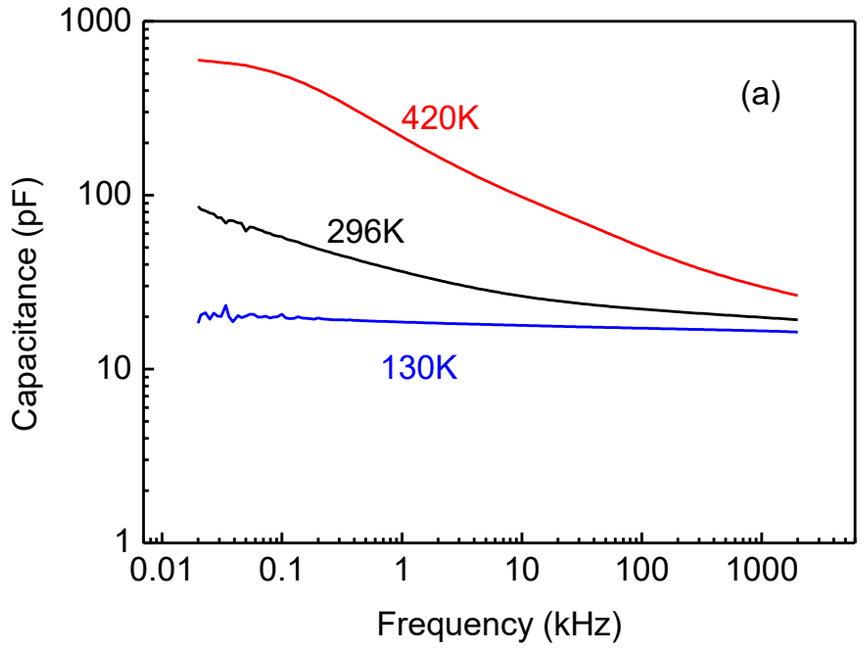

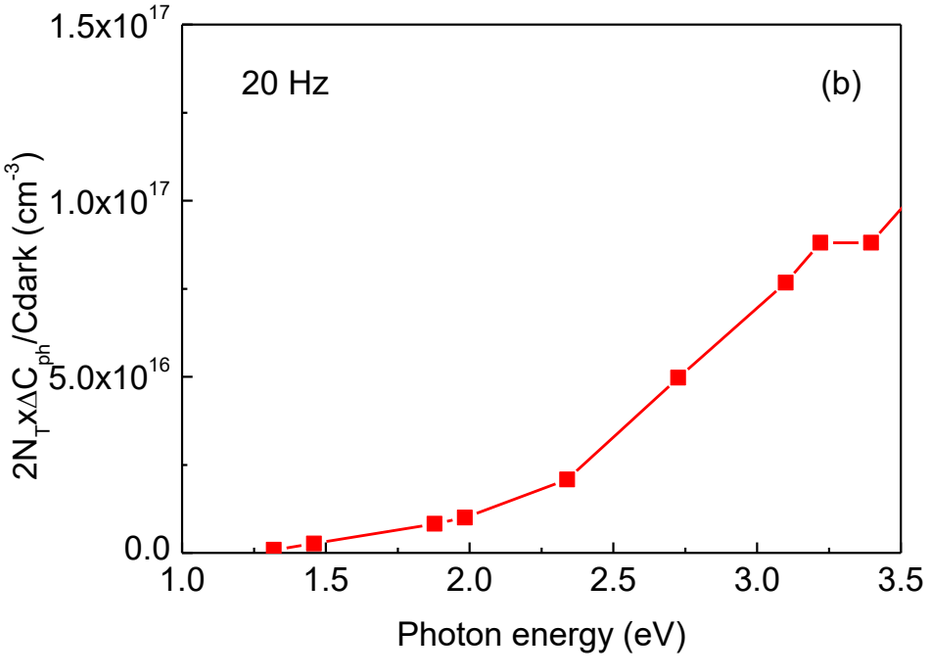

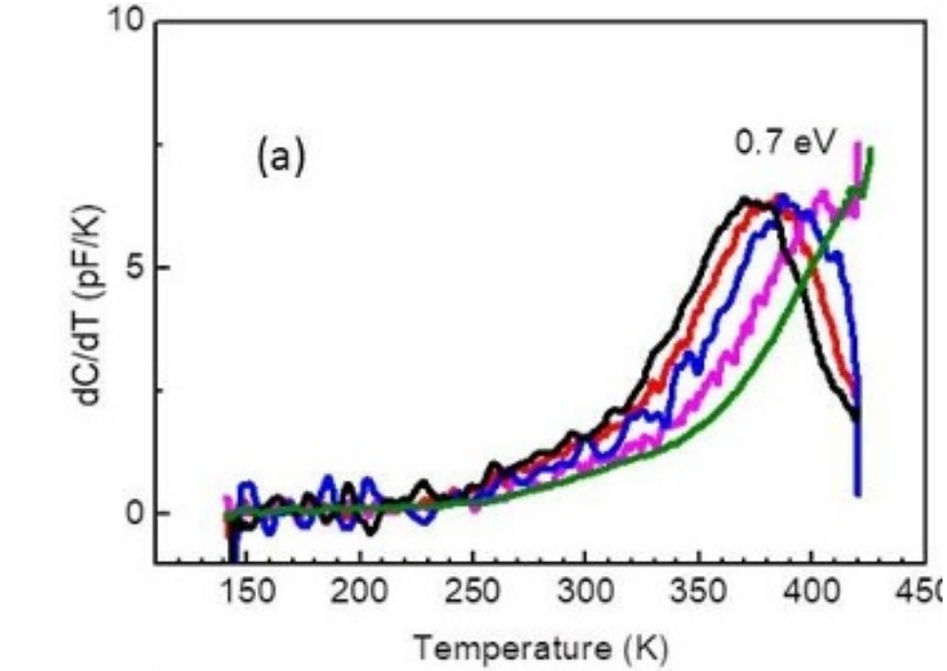

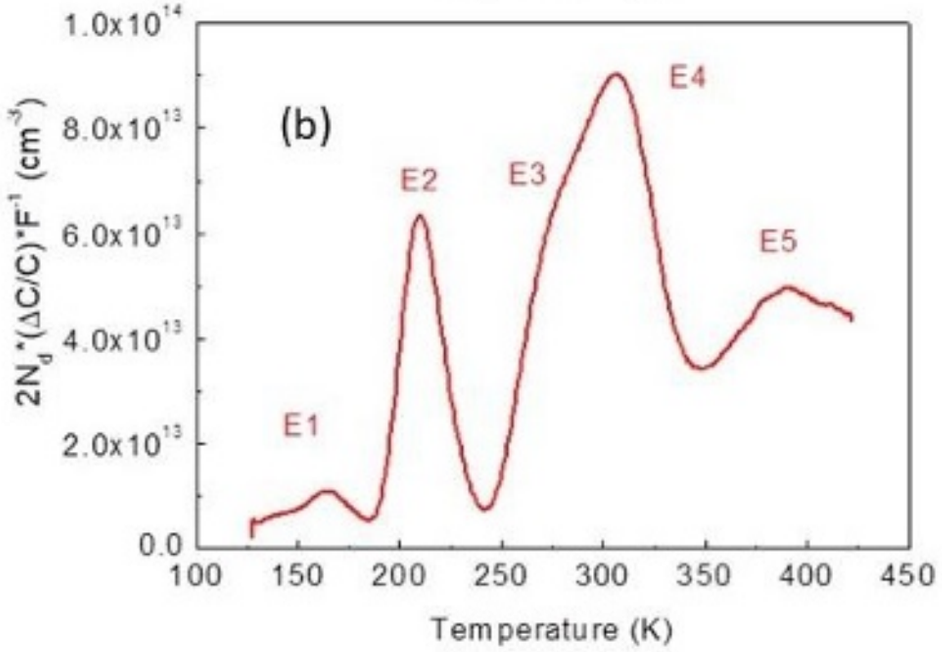

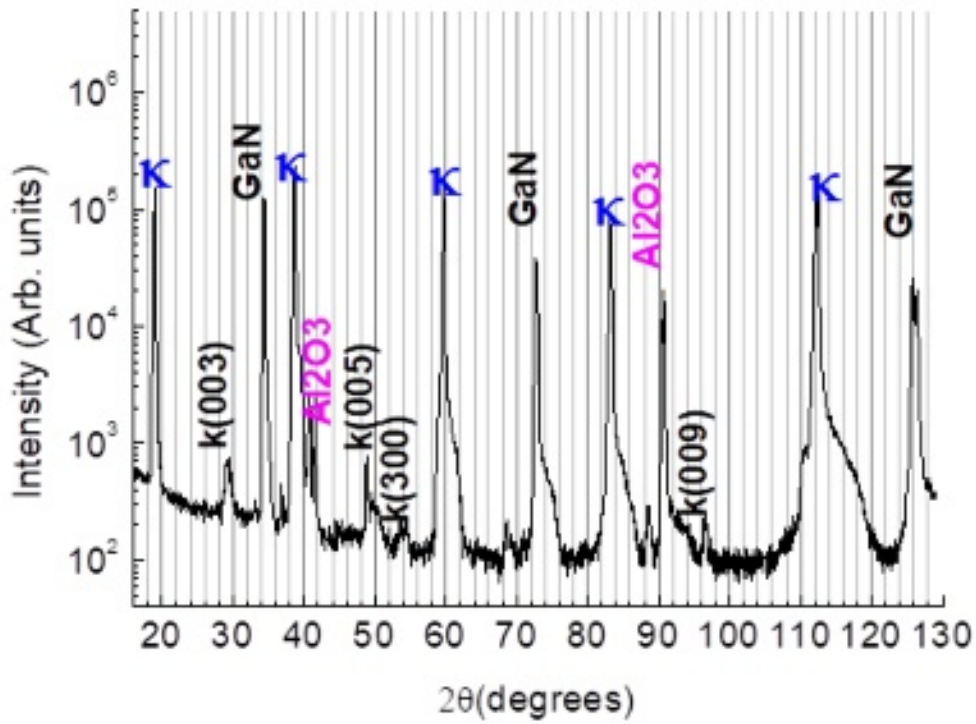
Intensity (Arb. units)
10^6
10^5
10^4
10^3
10^2
K
GaN
K
k(003)
Al2O3
k(005)
k(300)
K
GaN
K
Al2O3
k(009)
K
GaN
20 30 40 50 60 70 80 90 100 110 120 130
2θ(degrees)

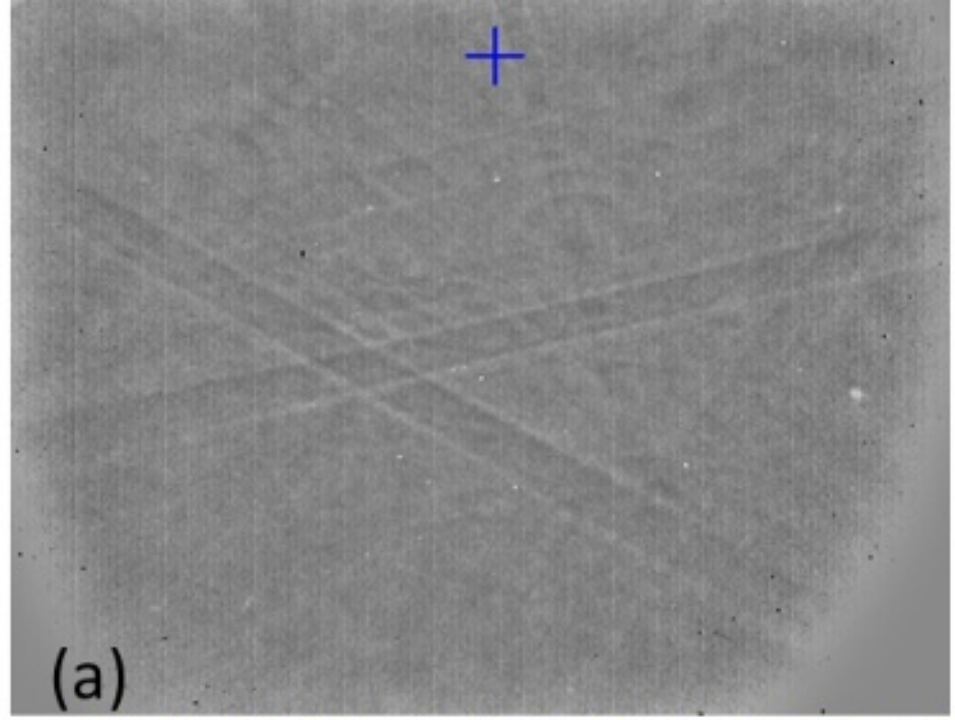
(a)

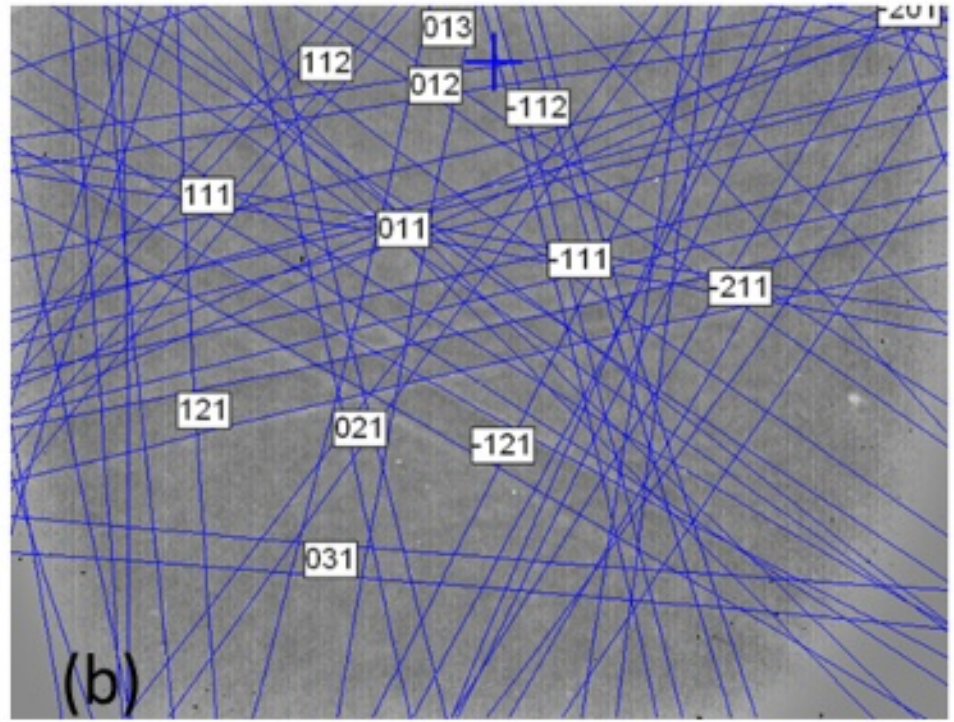
013
112
012
-112
111
011
-111
-211
121
021
-121
031
(b)

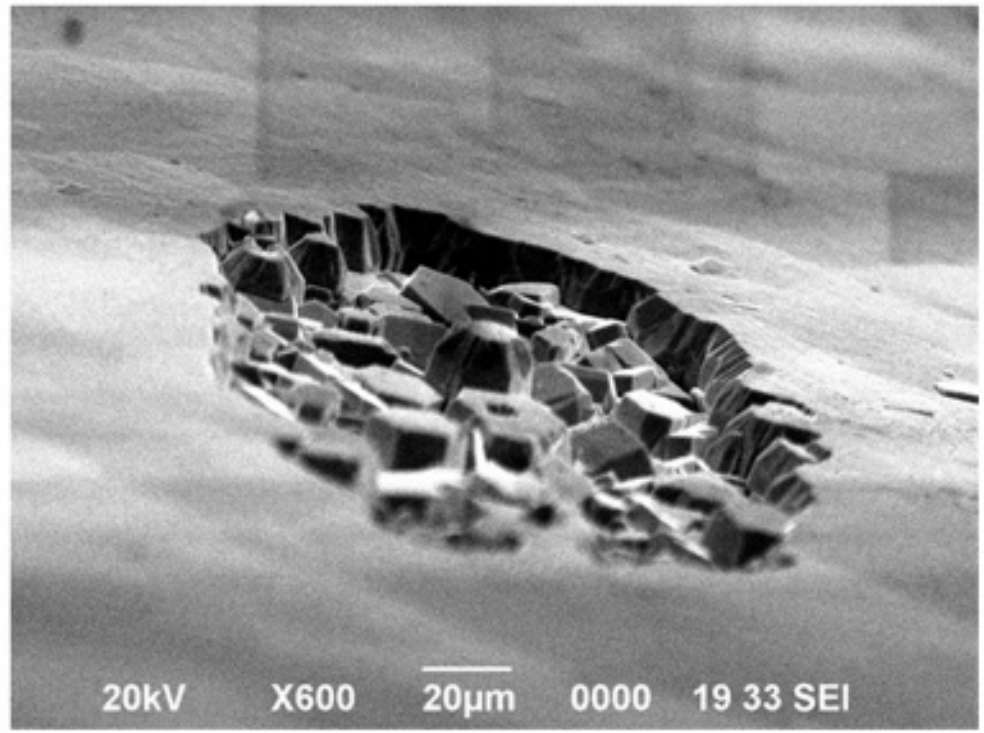
20kV X600 20µm 0000 19 33 SEI

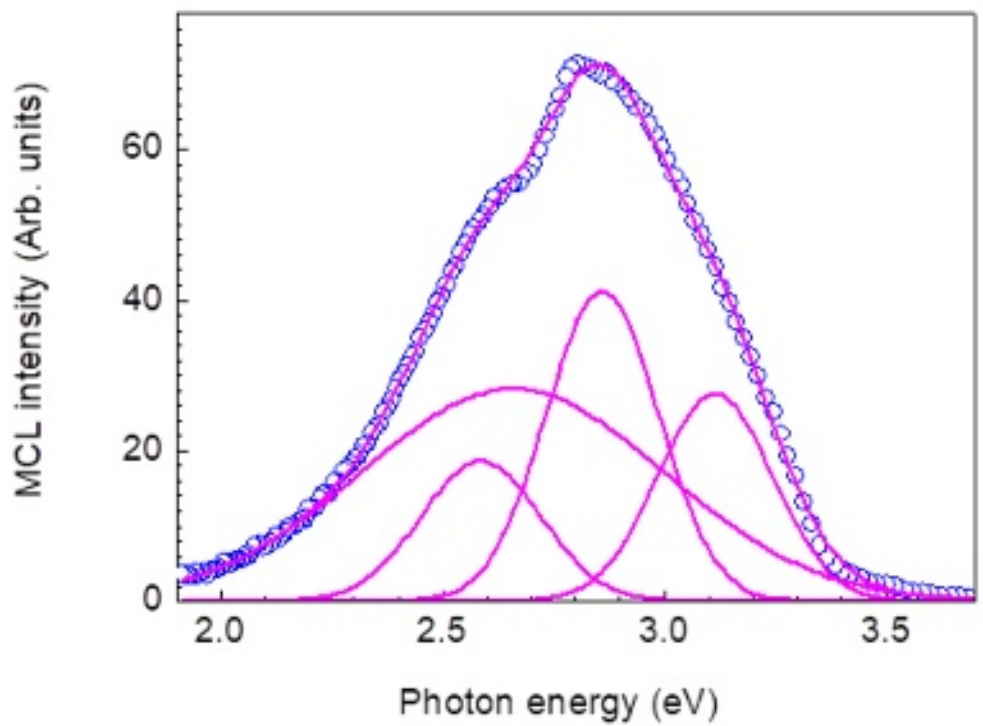
MCL intensity (Arb. units)
0
20
40
60
2.0
2.5
3.0
3.5
Photon energy (eV)

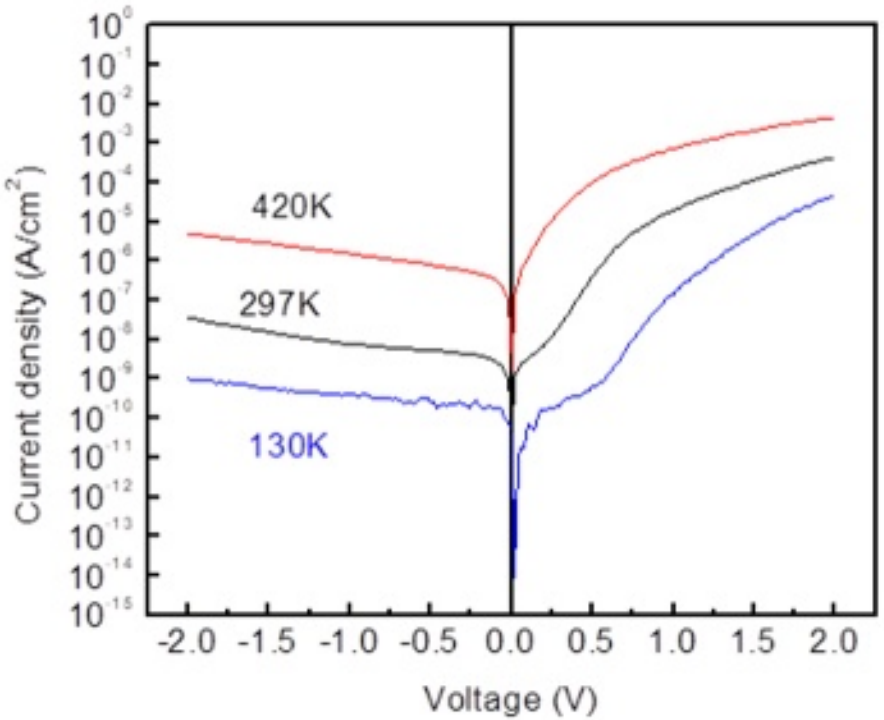
Current density (A/cm^2)
10^{0}
10^{-1}
10^{-2}
10^{-3}
10^{-4}
10^{-5}
10^{-6}
10^{-7}
10^{-8}
10^{-9}
10^{-10}
10^{-11}
10^{-12}
10^{-13}
10^{-14}
10^{-15}
420K
297K
130K
-2.0 -1.5 -1.0 -0.5 0.0 0.5 1.0 1.5 2.0
Voltage (V)

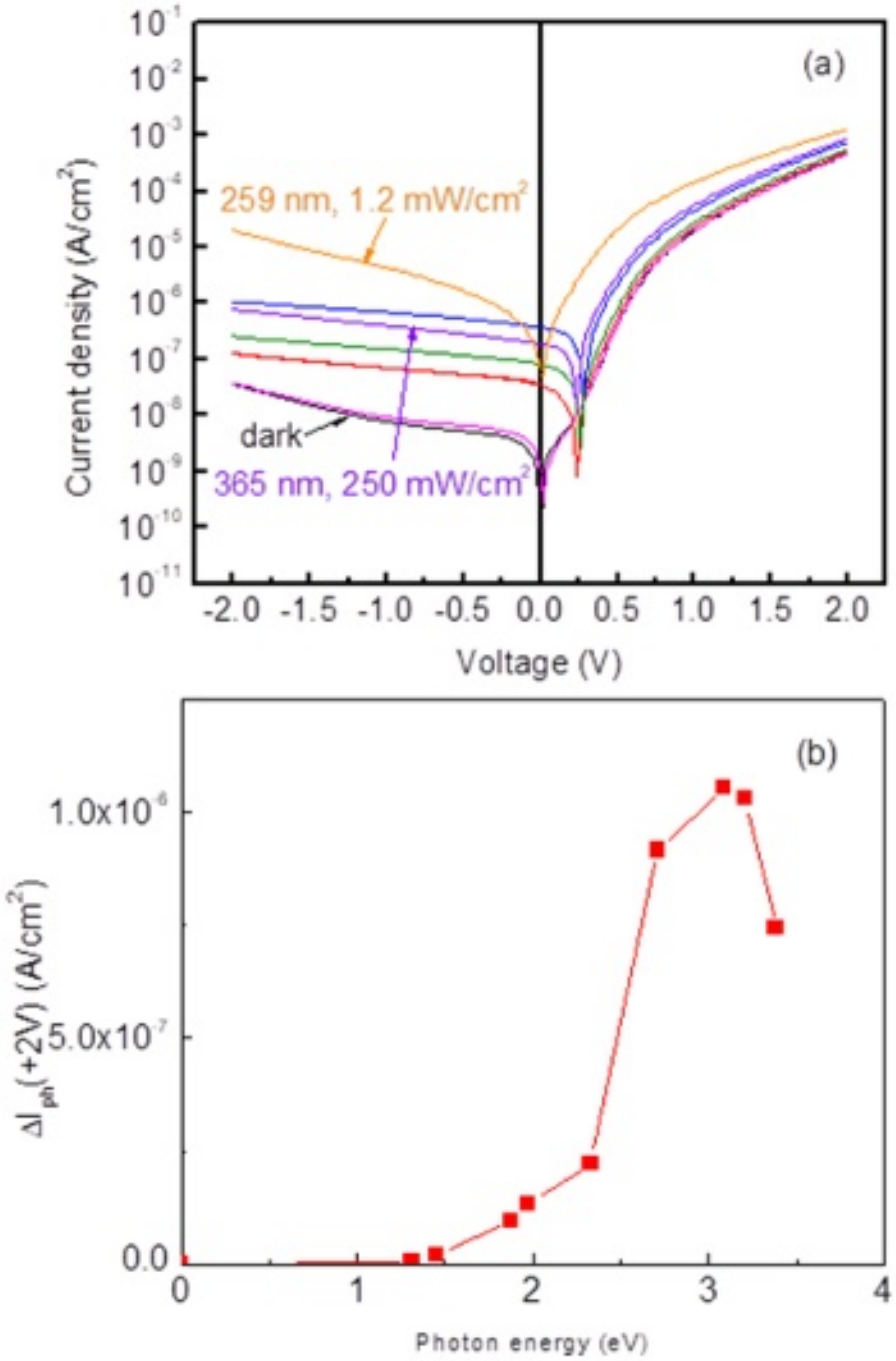
(a)
Current density (A/cm²)
259 nm, 1.2 mW/cm²
dark
365 nm, 250 mW/cm²
Voltage (V)
(b)
ΔI_ph(+2V) (A/cm²)
Photon energy (eV)

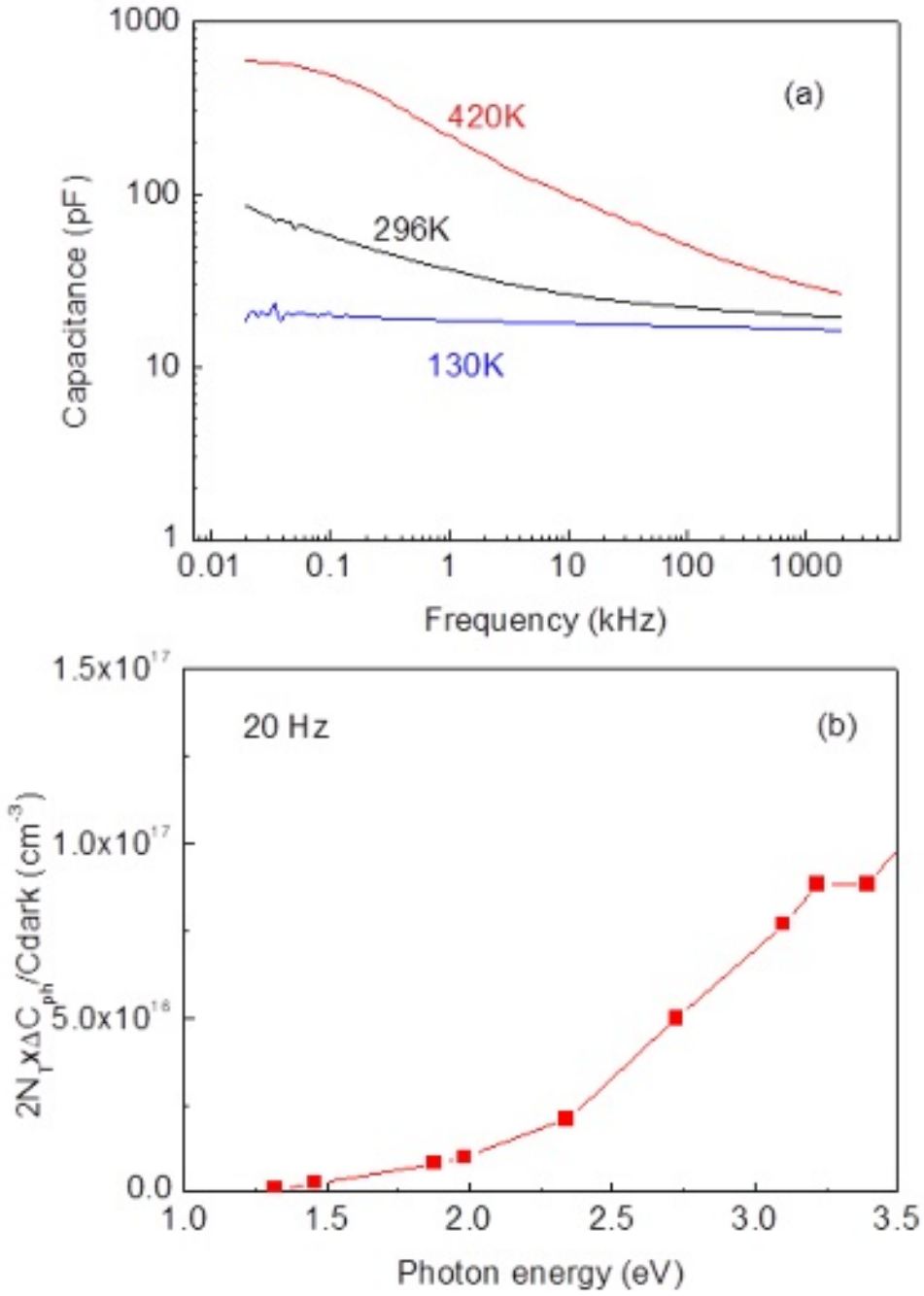
1000
100
10
1
Capacitance (pF)
420K
296K
130K
(a)
0.01
0.1
1
10
100
1000
Frequency (kHz)
1.5x10^17
1.0x10^17
5.0x10^16
0.0
2N_T xΔC_ph/Cdark (cm^-3)
20 Hz
(b)
1.0
1.5
2.0
2.5
3.0
3.5
Photon energy (eV)

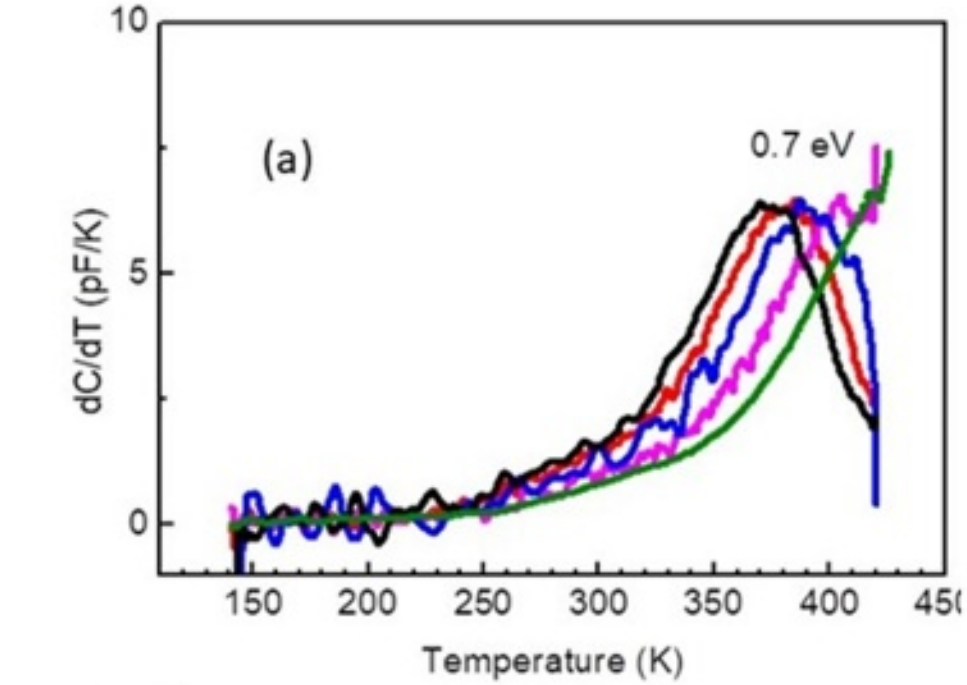
(a)
0.7 eV
dC/dT (pF/K)
10
5
0
150
200
250
300
350
400
Temperature (K)

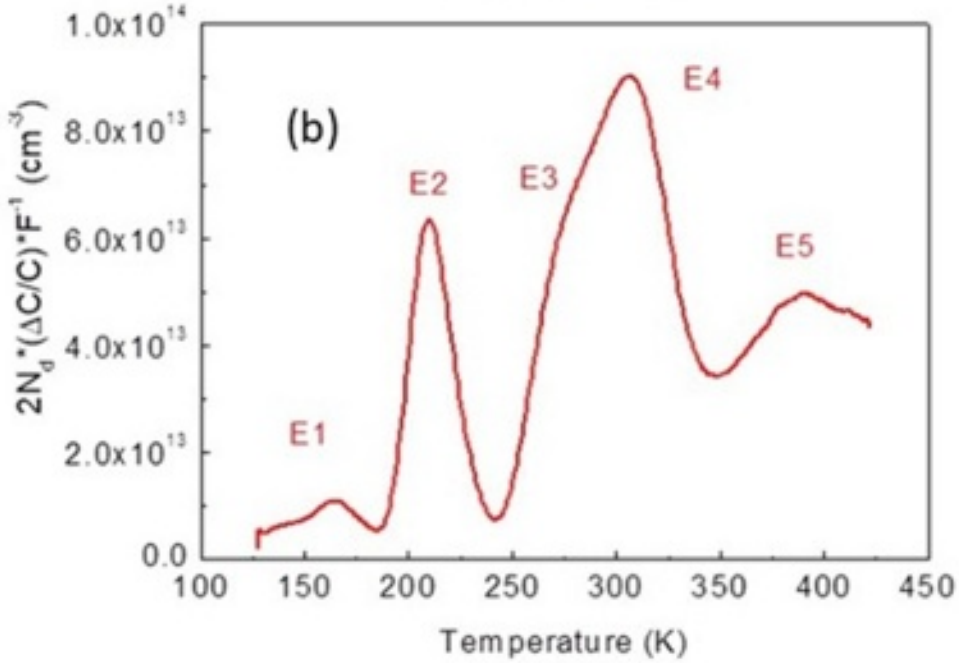
(b)
E1
E2
E3
E4
E5
$2N_d^*(\Delta C/C)^*F^{-1}$ (cm^{-3})
$1.0x10^{14}$
$8.0x10^{13}$
$6.0x10^{13}$
$4.0x10^{13}$
$2.0x10^{13}$
0.0
100
150
200
250
300
350
400
450
Temperature (K)